Internship report

ICFP Master - Quantum Physics

Nano-optics team - Laboratoire de Physique de l'Ecole Normale Supérieure de Paris

Broadband photodetection of the 2D semimetal $PtSe_2$

Author:
Esteban Foucher

Supervisors:
Assoc. Prof. Emmanuel Baudin
PhD student Marin Tharrault

2022 - 2023

CONTENTS

A. Introduction 3
B. Physical properties of the 1L-Bulk 2D material $PtSe_2$ 3
C. Fabrication of $PtSe_2$ field-effect transistors 4
1. Gold-assisted exfoliation of $PtSe_2$ 4
2. Hexagonal Boron Nitride encapsulation 6
3. $PtSe_2$ devices 7
4. Contact resistance 8
D. Conception of the ultrabroadband microphotodetection experiment 10
1. Photodetection setup 10
2. Computer interface 11
3. Charge damage protection 11
4. Control of the spot size 12
E. Photodetection results 13
1. Calibrated photodiode 14
2. $PtSe_2$ transistors 14
F. Conclusion 15
Acknowledgments 16

References 16

A. Introduction

Over the past two decades, 2D materials have emerged as very promising for advanced optoelectronics owing to their extraordinary optical absorption and very good transport properties. In addition to exhibiting high performances, their features (doping, gap, transport) are highly depandent on their environment (electric field, dielectric environment), and therefore this environment can be engineered offering unprecedented flexibility.

The 2D materials are a broad class of materials which contains the well-known semimetallic graphene and insulating hexagonal Boron Nitride, but also the semiconducting transition metal dichalcogenides (TMDCs) of interest for logic field-effect transistors and optoelectronics. The research efforts on TMDCs started with the thorough investigation of group-6 TMDCs (MoS_2, $MoSe_2$, $MoTe_2$, WS_2, WSe_2), which have the advantage of being easily exfoliable and having a NIR-VIS direct bandgap in the monolayer form. The group-10 TMDCs ($PtSe_2$, PtS_2, $PdSe_2$, PdS_2) is younger but saw a surge of interest motivated by their potential use in telecom technology. Indeed, the 1.55 μm central wavelength for long range fibered communications requires bandgap smaller than 0.8 eV which is reached by using a noble transition metal (Pt, Pd).

Comparatively to group-6 TMDCs, group-10 TMDCs are harder to exfoliate but easier to grow by various methods. This explains why past studies have been performed on low quality polycristalline $PtSe_2$, and already demonstrated remarkable performances for photodetection. In this work I introduce the study of intrinsic $PtSe_2$ photodetectors obtained by a gold-exfoliation method.

B. Physical properties of the 1L-Bulk 2D material $PtSe_2$

Cristalline structure - See Figure 1. PtSe2 occurs naturally in the 1T phase with an AA van der Waals (vdW) stacking of hexagonal layers. Pt atoms are in tilted octahedral sites and surrounded by 6 Se atoms (electronic structures: Pt : $[Xe]4f^15d^96s^1$ / Se : $[Ar]3d^{10}4s^24p^4$). The first brillouin zone of $PtSe_2$ is an hexagon reducible to the ΓMK triangle.

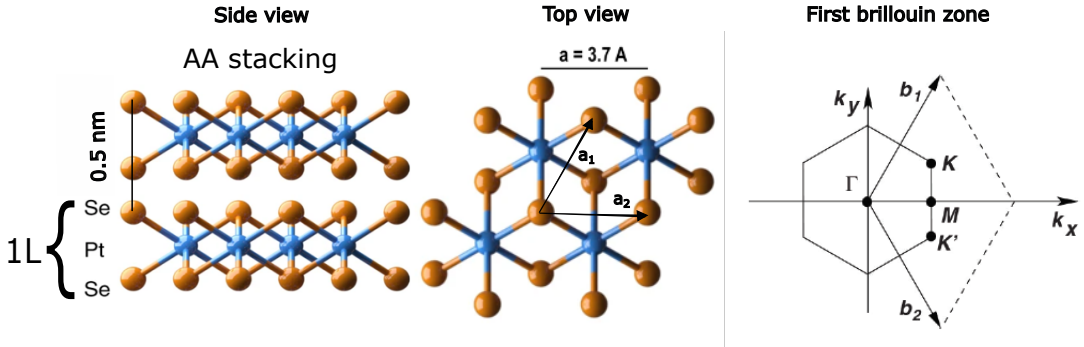

Figure 1: Se atoms are in yellow, Pt atoms in blue. **Left** : Side view. AA stacking of two layers of $PtSe_2$. Each layer is composed of three planes, two of Se atoms and one of Pt in between. All three planes are covalently bond. Interlayer cohesion is ensured by vdW interactions. **Middle** : Top view. Hexagonal structure of $PtSe_2$ layers. **Right** : Hexagonal first brillouin zone of $PtSe_2$.

The measured carrier mobility of $PtSe_2$ is of about 350-500 cm^2/Vs (measured by THz spectroscopy at DTU by Peter Bøggilde, private communication) which is high compared to other TMDCs. A comparative graph can be found in Figure 2a. $PtSe_2$ also exhibits excellent air stability.

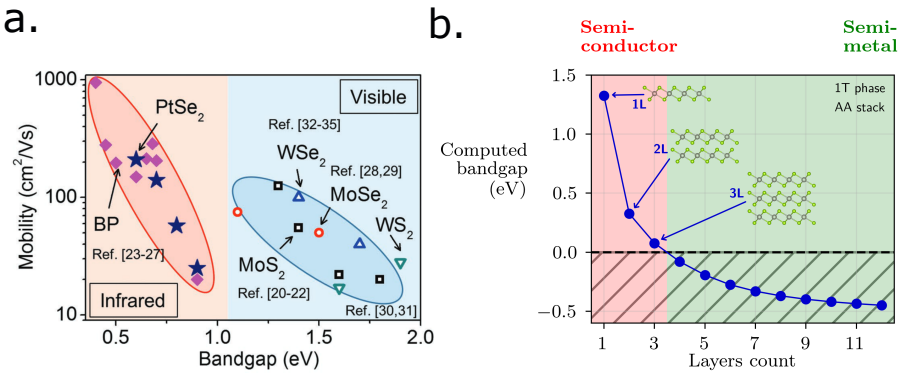

Figure 2: **a.** Previously measured mobilities and bandgaps of various 2D materials (from [6]). Today $PtSe_2$ measured mobility is higher than expected : 350-500 cm^2/Vs. **b.** Evolution of $PtSe_2$ bandgap as a function of the layer count computed by DFT using the independent particle approximation. The bandgap decreases as the number of layers increases. $PtSe_2$ thus exhibits a semiconducting behavior in below-4L forms and is semimetallic in thicker forms.

Like other TMDCs, $PtSe_2$ bandgap is thickness-dependent due to strong interlayer vdW interaction and can be tuned over the 0-1.3 eV range (see in Figure 2b). Band structures computed by DFT are represented on Figure 3. $PtSe_2$ is semiconducting from its 1L to its 3L form with decreasing bandgap and is semimetallic in thicker forms. This feature makes it an excellent candidate for 1-2 μm IR photodetection as one could stack several detectors with various thicknesses to cover the whole spectral range.

For a monocristalline $PtSe_2$ transistor, the expected mechanism for photodetection is the photoconductive effect : illumination promotes electrons from the valence band to the conduction band thereby increasing the total charge carriers density and thus the conductivity of $PtSe_2$. To have the best photodetection at a given wavelength we need good absorption, long carrier lifetime, and high electronic mobility. Absorption is not modified by the number of layers (not shown, M. Tharrault private communication), carriers lifetime is longer for semiconductors, but electronic mobility is higher for semimetals. Therefore, for a gap energy smaller than the application photon energy aimed, the best thickness is the result of a trade-off.

C. Fabrication of $PtSe_2$ field-effect transistors

To study intrinsic $PtSe_2$ photoresponse we need to fabricate devices. In this section we present how to exfoliate $PtSe_2$ wich is the core of the device, we then present results on the hBN encapsulation of $PtSe_2$, after we present the field-effect transistor geometry we chose for our devices and how to fabricate them, finally we present the devices obtained and the results about the contact resistance on thick $PtSe_2$.

1. Gold-assisted exfoliation of $PtSe_2$

$PtSe_2$ is hard to exfoliate due to its strong interlayer interactions, about 10 times stronger than graphite's. Standard mechanical exfoliation is thus unsufficient to obtain monolayer flakes with suitable size for optical studies. I thus used a gold-assisted exfoliation technique [4] to do so. This newly developped method relies on the good affinity between gold and Selenium atoms of $PtSe_2$ compared to the

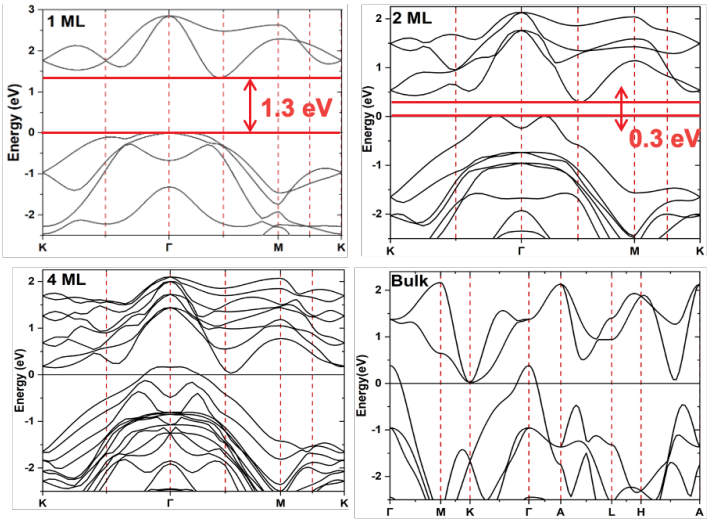

Figure 3: Band structures from DFT of 1L, 2L, 4L and bulk PtSe. For 1L and 2L $PtSe_2$ the valence band maximum is under the conducting band minimum, showing a semiconducting nature. For 4L and bulk $PtSe_2$ however, the VBM becomes higher than the CBM, showing a semimetallic nature.

interlayer vdW interactions. Depositing a gold layer on top of $PtSe_2$ enables the selective peel-off of a thin $PtSe_2$ film down to the monolayer.

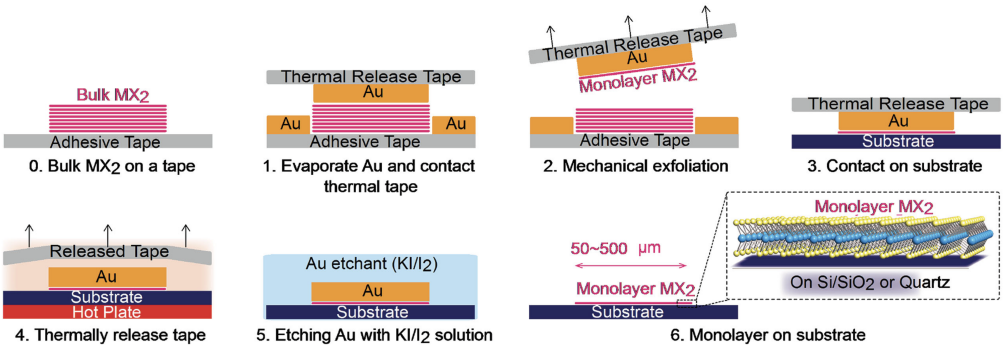

Figure 4: Adapted from [3]. Gold-assisted exfoliation scheme of an arbitrary MX_2 monolayer. **0-1.** Gold is evaporated onto a pre-exfoliated bulk crystal of MX_2. It is briefly heated at 150°C. Then thermal release tape is added on top. **2.** Mechanical peel-off of the topmost layer of MX_2. **3.** Contact on the final SiO_2/Si substrate. **4.** Thermal release of the tape. **5.** Chemical etching of the residual gold film in a KI/I_2 solution.

Protocole (see scheme in Figure 4 adapted from [3]) :

1. Gold is evaporated onto a pre-exfoliated bulk crystal of $PtSe_2$.

2. A thermal release tape is used to peel-off the topmost $PtSe_2$ layer and is then stuck on the final SiO_2 substrate.

3. The tape is then realeased at 130°C and the residual gold film is selectively etched in a KI/I_2 solution.

Additionally, at LPENS a heating at 150°C is added between step 1 and step 2 to improve yield of the exfoliation at the peel-off stage. The differential dilation of gold and $PtSe_2$ results in a mechanical stress at their interface weakening interlayer interactions. This allows to obtain flakes of the order of 10μm with acceptable yield. This lateral size is much larger than the diffraction limit of the microscope resolution thereby allowing quantitative optical study. Some examples I obtained using this technique are pictured in Figure 5. Mastering gold-assisted exfoliation has been a key asset for the LPENS to overcome the fabrication challenge and lead pioneering investigations on ultra-thin $PtSe_2$ properties.

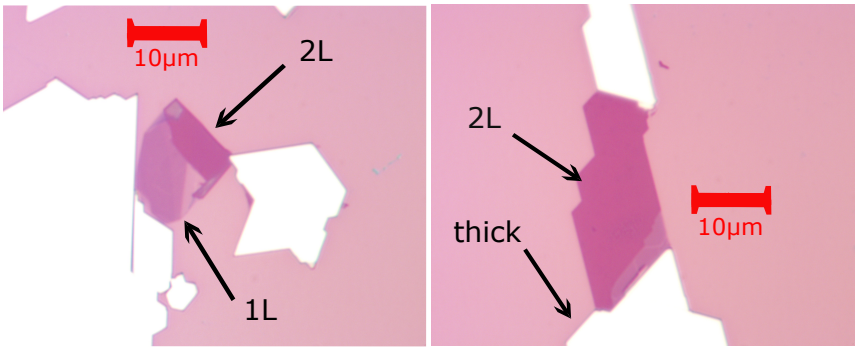

Figure 5: Scalebars = 10μm. $PtSe_2$ flakes on a 280nm SiO_2/Si substrate. Pictures taken on the microscope at x100 magnitude.

2. Hexagonal Boron Nitride encapsulation

$PtSe_2$ samples obtained with gold-exfoliation technique present excellent optical and transport properties. However, it is well-known that hBN-encapsulation improves vastly 2D materials physical properties allowing to reach the intrinsic regime [1]. This is because hBN is an excellent dielectric insulating environment, and hBN encapsulation naturally "cleans" the TMDC surfaces from chemical polluants.

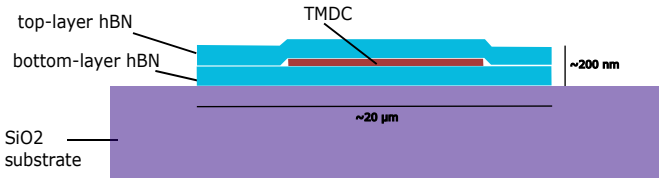

Figure 6: Schematic diagram of the aimed hBN encapsulated TMDC structure (side view).

I thus tried to encapsulate a monolayer $PtSe_2$ flake, the aimed structure is sketched in Figure 6. The process (described in Figure 7) failed because the adhesion of the TMDC to the top hBN flake was not sufficient to detach it from the SiO_2/Si substrate. This has two explanations :

First, the surface of the $PtSe_2$ flake could be chemically polluted by the KI/I_2 solution used during final gold etching.

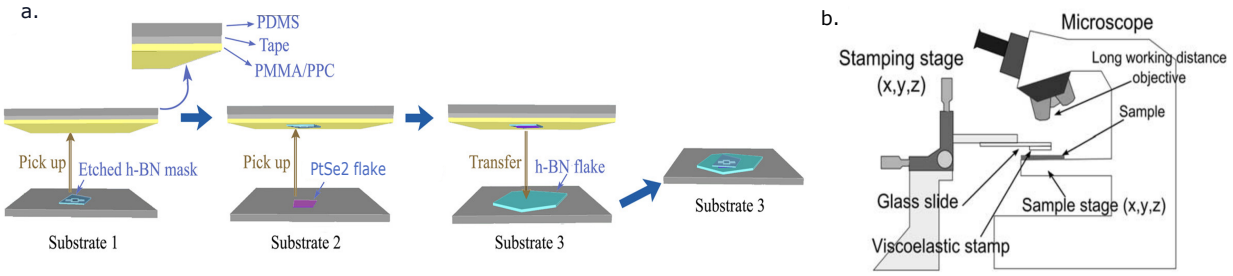

Figure 7: **a.** Adapted from [5]. Schematic diagram of the steps needed for the hBN encapsulation of a TMDC. A first top-layer hBN flake is picked up with the viscoelastic stamp. Then the core TMDC flake is picked up and stacked under the top-layer hBN on the stamp. Finally the stack is transferred on the bottom hBN flake. Contrarily to the diaram, we used a droplet of PDMS coated with PPC as a viscoelastic stamp. Its curved shape allows the selective pick-up of a user-defined area on the substrate. **b.** Adapted from [2]. Schematic diagram of the experimental setup employed for the encapsulation process.

Second, the peeled thin $PtSe_2$ on Au layer is fragile and could experience damaging mechanical stress during peel-off and substrate deposition. This study reveals a limit of the Au-assisted exfoliation technique which, if lifted, could greatly enhance the flexibility in the fabrication of high-quality devices.

3. $PtSe_2$ devices

Having prepared the raw 2D material, the next step consists in fabricating a device out of it for use in photodetection. This section describes the geometry of $PtSe_2$ field-effect transistors (FETs) to be studied in the photodetection experiment, their fabrication protocole, and the results we obtained on the electrical contacting of thick $PtSe_2$.

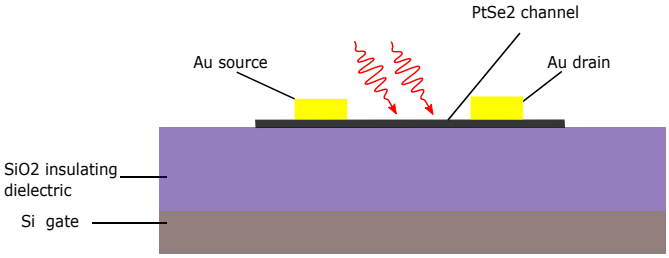

Figure 8: Geometry of a $PtSe_2$ FET. In black, the $PtSe_2$ channel where current flowing provoked by applying a bias voltage on metallic (Au) contacts. The capacitance geometry of the channel and Si backgate with a 90nm SiO_2 spacing as insulator enables to dope the channel.

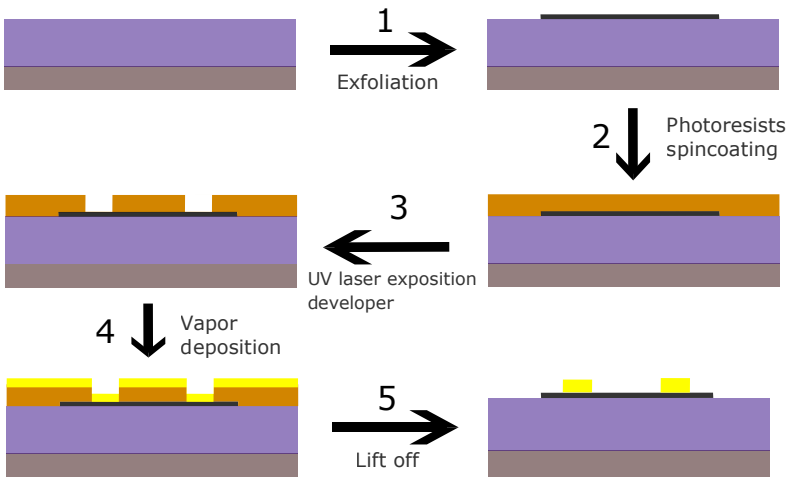

Figure 9: Fabrication scheme of a FET. **1** Exfoliation of the TMDC. **2** Spincoating of the positive photoresist. **3** Laser lithography defines the geometry of the future contacts. Development : selective etching of UV exposed areas of the photoresist. **4** 160nm thick metallic deposition of contacts. **5** Lift-off in acetone.

Device geometry - Our devices (see Figure 8) are field-effect transistors (FET). This geometry enables to control the doping of the TMDC channel. Indeed the Si backgate and the $PtSe_2$ channel form a capacitance of area $3\mu m \times 3\mu m$ spaced with SiO_2 on a thickness $t_{SiO2} = 90nm$. The capacitance by surface unit is thus $c_g = \frac{\epsilon_0 \varepsilon_{SiO2}}{t_{SiO2}} = 490\mu F.m^{-2}$, taking the relative dielectric permittivity of SiO_2 $\varepsilon_{SiO2} = 5$. The doping of the channel is thus $n = 3.1.10^{11} cm^{-2}$. Source and drain metallic contacts allow applying a bias (typically few 10s of mV), provoking a current flow.

Fabrication scheme - In this paragraph we detail the lithography process to fabricate a FET (See Figure 9) :

- Step 1 is the gold-assisted exfoliation of $PtSe_2$ (See section C 1).
- Step 2 is the spincoating with a positive photoresist (AZ 5214E) and 2 min bake at 110°C of activation.
- Step 3 is laser exposure to define the contact geometry. Only areas exposed to UV light are selectively etched in the developer (AZ 400K (1:4) solvent).
- Step 4 is the metal deposition of the contacts (5 nm Cr adhesion layer and 180 nm Au layer). To test contact performances we chose to make devices with and without chromium layer.
- Step 5 is the lift-off in acetone : all the remaining photoresist is removed.

4. Contact resistance

In this paragraph we present 2 semimetallic transistors we fabricated and their transport and gating properties (see Figure 10).

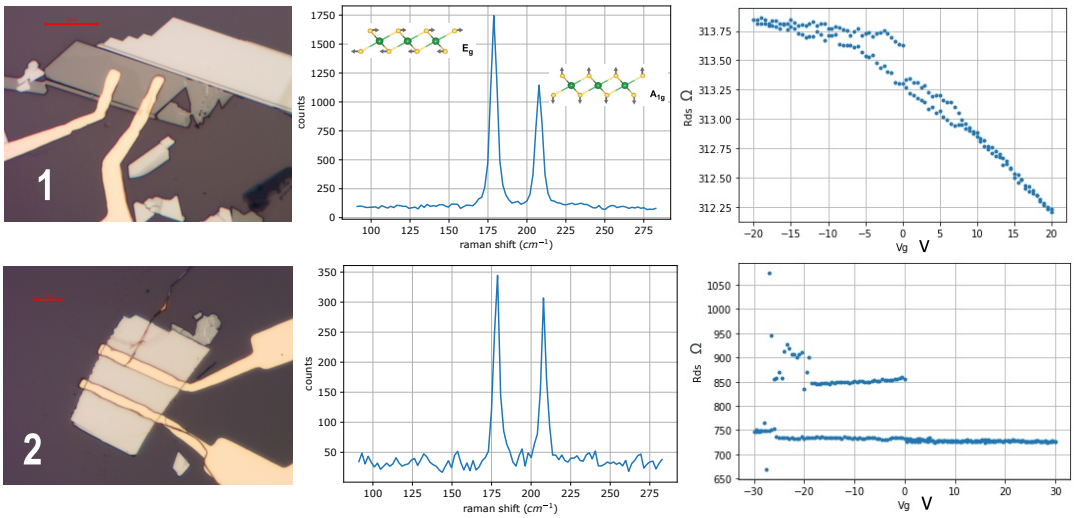

Figure 10: **Left :** The two fabricated $PtSe_2$ FETs pictures observed on the microscope. Scalebars = 10 μm. **Middle :** Their raman spectra. The size ratio of the peaks E_g and A_{1g} indicates transistor n°1 channel is 12L-thick $PtSe_2$ while transistor n°2 is much thicker. **Right :** Measured drain-source resistance function of gating. Transistor n°1 exhibits a weak field effect (0.2%). Transistor n°2 has no vsible field effect. Its drain-source resistance curve presents a measurement artifact.

Transistor n°1 is made of a 5.5μm-large $PtSe_2$ channel with Au contacts. Raman spectroscopy indicates that it is about 12 layers-thick. The 313 Ω drain-source resistance is good compared to the typical MΩ contact resistances for group-6 TMDCs. It exhibits a weak field effect (0.2 %) with the gating. We actually measure the total of the two contact resistances and the channel resistance that form a voltage divider. However, the fiel effect only modulates the channel resistance. This mesured field effect indicates the preponderant channel contribution in the resistance with respect to contact resistances, which values are probably under the order of 10Ω.

Transistor n°2 is a much thicker 10 μm-large $PtSe_2$ channel with Cr/Au contacts. Its drain-source resistance is 740 Ω. The contact quality is poorer and the flake is too thick to exhibit field effect.

We ultimately want to study thin semiconducting $PtSe_2$ photodetectors. However, contact resistance on PtSe2 must be as low as possible to enable sensitive measurement. One difficulty is that - as for all TMDCs - it is very hard to obtain low contact resistance on semiconducting $PtSe_2$. Indeed, the bandgap of $PtSe_2$ is prone to develop a Schottky barrier at contact therefore limiting the channel current.

$PtSe_2$ bandgap flexibility offers an elegant solution to the contact problem : thick semimetallic $PtSe_2$ above the thin semiconducting $PtSe_2$ channel can be used as precontact and contacted with gold. My study aimed at minimizing this Au-$PtSe_2$ contact resistance. The above results indicate that contact resistances on semimetallic $PtSe_2$ are good compared to the typical 50 MΩ contact resistance measured on bilayer $PtSe_2$ by the team.

In the following those FETs will also constitute test devices in photodetection.

Having now prepared $PtSe_2$ photodetectors it is now time to explain how to measure their photoresponse.

D. Conception of the ultrabroadband microphotodetection experiment

To study the photodetection response of $PtSe_2$ transistors, I built an ultrabroadband microphotodetection experiment described in this section. The section discusses the main tasks it involved : the computer interfacing, the development of charge damage protections of the devices, and spectral focus shift calibration measurements. With $PtSe_2$ devices we expect to observe a response due to photoconductive effects, where illumintation promotes charge carriers and thus increases the conductivity.

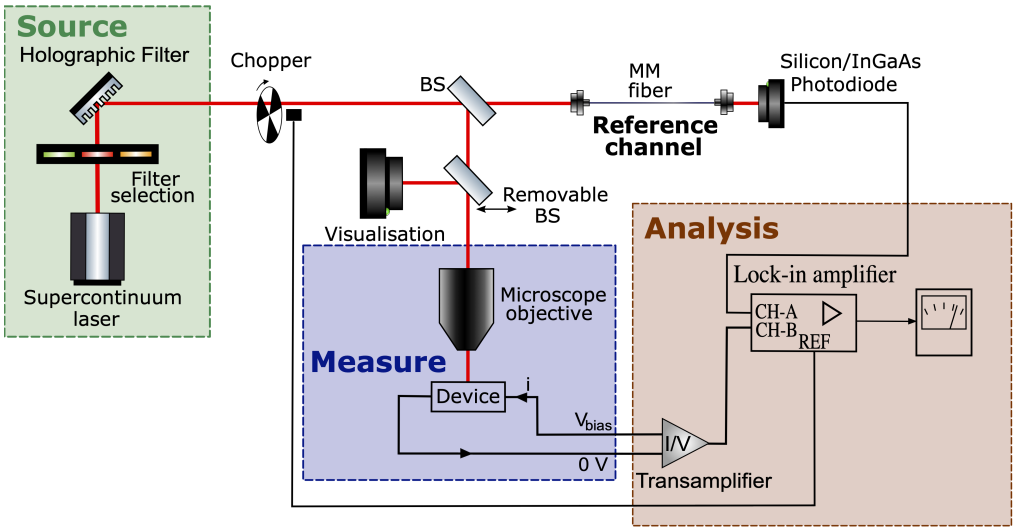

Figure 11: Diagramatic scheme of the photodetection setup. **Source -** For broadband, powerful and spatially coherent light we use a supercontinuum laser. The excitation wavelength is selected with a holographic filter. Additionnal filters are used to prevent higher orders diffraction parasite light from the holographic filter. **Measure -** In the main channel, light is focused on the device with an achromatic microscope objective. **Analysis -** We use a homodyne detection scheme relying on a lock-in amplifier and an optical chopper. The photocurrent signal from the device is amplified with a low noise transamplifier. An amplified photodiode is used as a reference to monitor the laser power. A removable beamsplitter enables visualization with the camera.

1. *Photodetection setup*

The photodetection setup scheme is presented on in Figure 11. All devices are remotely controlled by a computer using a python interface.

Source - The limited micrometric size of devices can only be investigated using nearly diffraction limited excitation spot size. To have broadband powerful and spatially coherent light we use a supercontinuum laser as a light source (Fianium Whitelase micro, 200 mW, 450-2000nm). We can select the excitation wavelength with two holographic filters (VIS : 400-850nm range / IR : 850-1700nm - Photon etc. LLFT Contrast). Additionnal bandpass filters are used to avoid higher order diffractions of the holographic filters.

Measure - In the main channel, light is focused on our device thanks to an apochromatic microscope objective (Mitutoyo M Plan APO SL 80x for VIS and M Plan APO NIR HR 100x for IR). We measure the resulting photocurrent in the device under drain-source bias voltage.

Analysis - To be able to detect the photocurrent at drain-source contacts with a large signal-to-noise ratio, we use a homodyne detection scheme relying on a lock-in amplifier (7265 DSP) along with an optical chopper that modulates illumination at 220Hz. Because the typical current generated in our devices is small (about few μA), the signal is amplified by a low-noise transamplifier (Femto DLPCA-200) with a transimpedance reaching 10^9 V/A. The laser power is monitored and used as a reference signal by using a beamsplitter on the excitation beam path and an amplified photodiode (VIS : Thorlabs PDA36A2, IR : Thorlabs PDA50D2). Finally, a removable beamsplitter enables vizualisation with the camera (Nikon D5500).

2. Computer interface

To control the whole experiment I wrote a computer interface in python code using an object-oriented programming structure. Each device of the experiment is defined as an object that can perform elementary tasks. A higher level class defines the whole photodetection experiment that controls all devices simultaneously. This structure is on Figure 12.

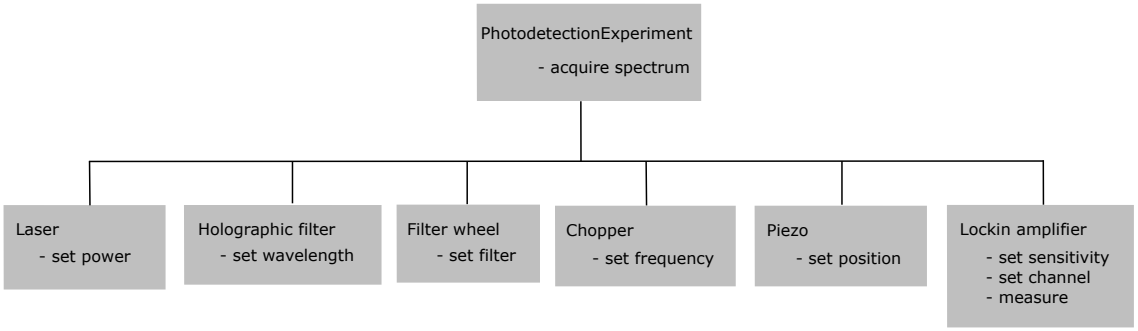

Figure 12: Diagram of the interface structure. Each box represents a python object that can execute elementary tasks.

3. Charge damage protection

Due to their small size, our devices are extremely sensitive to electrostatic discharges and ground issues that can damage them. Figure 13 pictures a pioneering device having experienced such fate.
The principal danger comes from the switching power supply of the transamplifier that generates leakage currents to the ground. To avoid current discharges through our device, the optical table is grounded and the case of the transamplifier is connected to the table. In addition, a removable resistive shunt is added on the device connector to dissipate potential charges accumulated in the circuit when connecting it. With theses precautions we did not experience damages on new devices.

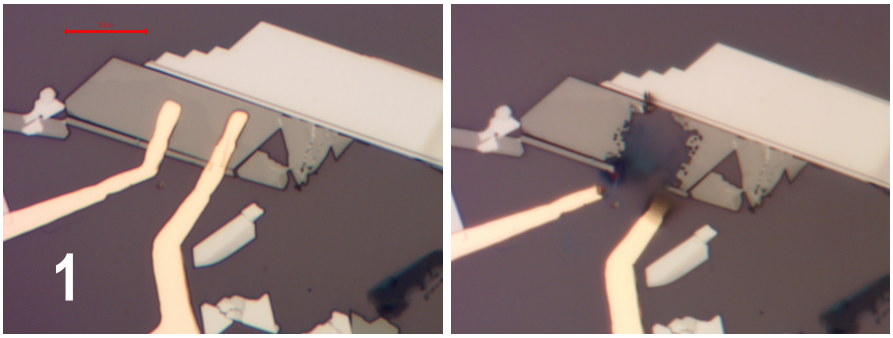

Figure 13: Damaged device, before and after connecting to the transamplifier.

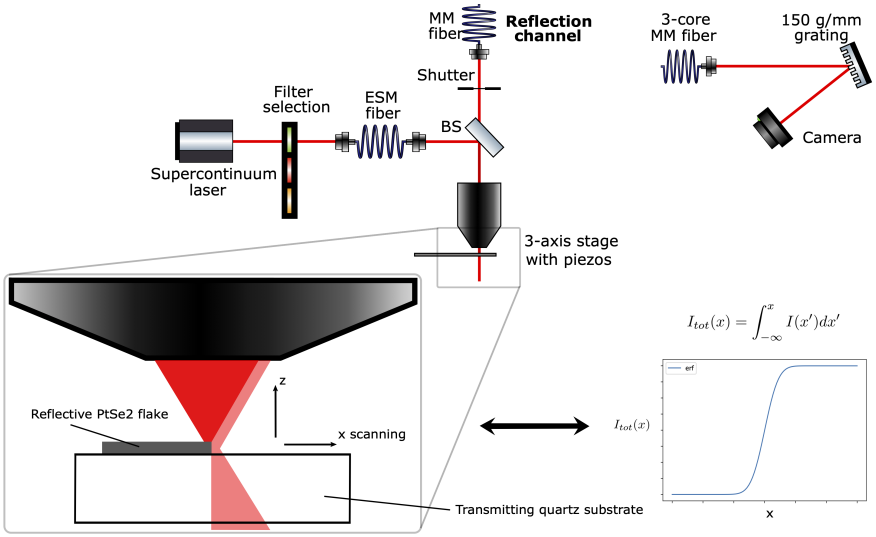

Figure 14: Knife-edge method setup and scheme. The lightbeam is scanned along the transverse x direction across the sharp edge of a reflective $PtSe_2$ flake. Reflected light is analyzed in a spectrometer over the full spectral range. The intensity as a function of x has an error function shape for a gaussian beam.

4. Control of the spot size

Quantitative characterization of our devices photodetection response requires the precise control of spot size. However, over the ultrabroad range explored, the microscope objective presents a few micrometers chromatic focus shift. I thus measured this effect over the whole spectrum using the knife edge method (see Figure 14).

Knife edge method - The knife edge is an optical method to measure the size of the lightbeam. It consists in measuring the transmitted or reflected light while scanning the beam along a transverse axis (x direction in Figure 14) across a sharp edge. I used a highly reflective $PtSe_2$ flake on a non-reflective quartz substrate. $PtSe_2$ flakes have very clean edges as they break along cristalline axis. The reflected light is analyzed in a spectrometer over the full spectral range. For a gaussian beam, the intensity of the reflected signal as a function of the tranverse axis coordinate takes the shape of an error function. We

analyzed our data using this model and repeated the operation for all focuses (z direction in Figure 14). We defined the origin of the optical axis ($z = 0$) as the optimal focus of the 650 nm component of the laser.

I successfully managed to measure this effect in the visible range (420-980 nm, see Figure 15). The chromatic focus shift ranges over a 6μm range on the whole visible spectrum (Figure 15c). From results pictured in the graph of the optical beam size function of focus at 3 wavelengths (Figure 15b), we can already state without implementing any correction of the focus shift effect that the beam size is always smaller than 1.5μm. However, taking this effect into account in the control interface of the experiment will ultimately be needed for fine control of the excitation intensity and illuminated area. Short exposure times (200 ms) required by the visible Si camera allowed reliable visible range measurements. However, the InGaAs camera for IR range has longer exposure times (2000 ms) and the thermal dilation of the optical setup limits measurements. Further minor work will be needed to overcome this issue.

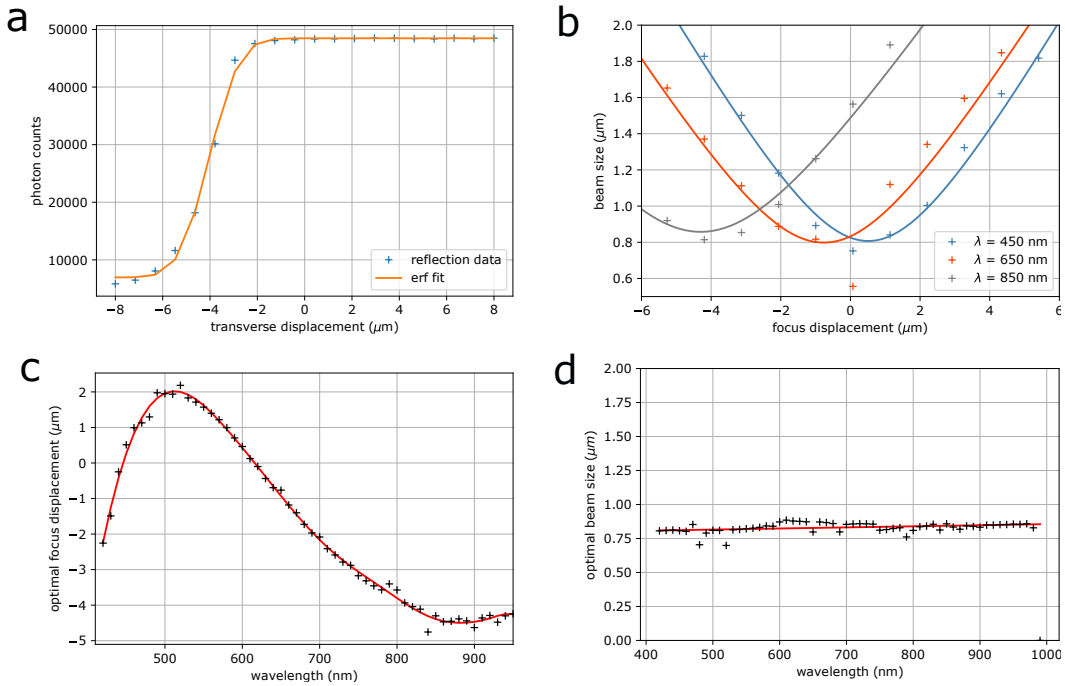

Figure 15: **a.** Intensity scan along transverse direction x fitted with an error function. **b.** Optical beam size function of focus at 450nm, 650nm and 850nm wavelengths. Fits are hyperbola functions. **c.** Chromatic focus shift in visible range. **d.** Optimal beam size function of wavelength.

E. Photodetection results

In our experiment we measure the photocurrent response at the drain-source contacts of our $PtSe_2$ device.

As the lock-in measurement isolates the first harmonic response, we can drop higher order terms of the square modulated incoming light and write its power as $P_\lambda(t) = P_{0\lambda}(1 - cos(\omega t))$ at first order. Accordingly, the current through the photodetector under illumination has the form $I_\lambda(t) = I_0 + \Delta I_\lambda cos(\omega t + \theta)$. I_0 is due to the bias applied to the drain-source contacts and ΔI_λ is the modulated photocurrent of in-

terest, measured by the lock-in in the form of a voltage $\Delta V_\lambda = R_{TA}\Delta I_\lambda$ after I/V transamplification, where R_{TA} is amplification resistance of the transamplifier.

Two main mechanisms can explain photoresponsivity. The first is photoconductivity : illumination increases the charge carriers density and thus the conductivity. This mechanism does not generate current and requires the device to work under the application of a bias voltage to be detected. In this case, the photoresponsivity $R_{PC}(\lambda)$ is defined as $\Delta V_\lambda = P_{0\lambda}V_{bias}R_{TA}R_{PC}(\lambda)$. Our $PtSe_2$ FETs are typical devices of this class.

The second is the photovoltaïc effect happening at junctions between p-doped and n-doped semiconductors, for example photodiodes used in the first subsection E 1. A current is actually generated in the device and is detected without bias applied. Here the photoresponsivity $R_{PV}(\lambda)$ is defined as $\Delta V_\lambda = P_{0\lambda}R_{TA}R_{PV}(\lambda)$. Preliminary results acquired with the photodetection experiment are described in this section.

1. *Calibrated photodiode*

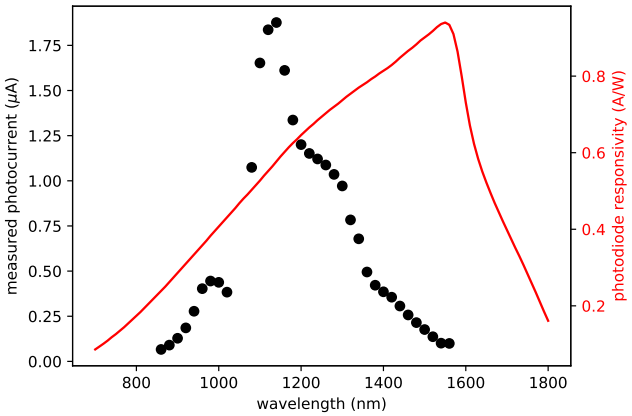

Figure 16: Calibrated photodiode photocurrent response function of wavelength (black dots). Measured with 0V bias. The rescaled responsivity profile (A/W) is added in red. Major shape differences are due to the laser chromatic power variations.

To measure absolute photocurrent responsivity, we make use of a calibrated photodiode as a reference (VIS : Thorlabs FDS100-CAL, IR : Thorlabs FDG03-CAL). This reference measurement is presented in Figure 16. These measurements are remarkably precise and stable (<1% precision). The difference in spectral dependence originates from the laser colour spectral power density. The comparison of the two curves indicates the excitation power on the device is of about a few μW.

2. *$PtSe_2$ transistors*

I first did measurements of the $PtSe_2$ photoresponse. The first device was damaged when connected to the transamplifier (see section D 3). However I could acquire an IR spectrum on the second transistor of section C 3 (see Figure 17).

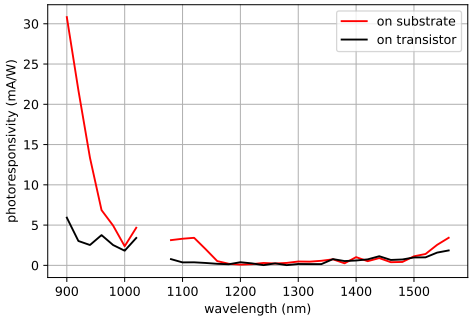

Figure 17: Thick $PtSe_2$ transistor photoresponsivity with 50mV drain-source bias. $22k\Omega$ drain-source resistance. IR photodetection spectrum taken on the 90nm SiO_2 substrate (red) and on the device (black). We observe a general cut-off of the responsivity at around 1000nm while on-substrate measured responsivity is much higher than on device.

Substrate response - The curves (Figure 17) show a clear decrease around 1000 nm, which is characteristic of the silicium bandgap. Moreover, the signal is larger when light hits the substrate than when it hits the transistor. We conclude that the photodetective effect from the Si substrate dominates the device response while the transistor is only masking the substrate. This important result shows a limit to the Si backgate geometry and that other substrates like Quartz or Saffire should be considered for further FET fabrications.

To be improved - Some other factors can explain why we cannot measure a response. When fabricating the millimetric contacts needed to connect the device, the latter's total resistance uncommonly increased from 750 to 22kΩ. This results in a signal reduction by a factor 70 compared to the 300 Ω obtained with transistor n°1. While our device was a 10μm $\times$ 10μm square channel, this surface should be reduced close to the excitation spot size to maximize the illuminated surface of the channel and incident intensity. A 3 μm square channel should optimal, just being large enough not to expose the contacts to light. Finally, the device is probably too thick so that light induced pair creation originates vastly on the top surface. Therefore the parallel conductance of the bulk $PtSe_2$ underneath shortcuts the photodetection signal.

F. Conclusion

This work involved the fabrication of $PtSe_2$ devices and the development of a photodetection experiment. Using a new Au-assisted exfoliation technique, we built transistors and checked semimetallic $PtSe_2$ was easily contactable. We furthermore tried to encapsulate a $PtSe_2$ monolayer and it revealed an adhesion limitation of the $PtSe_2$ and the hBN coming from the exfoliation technique. We did preliminary tests of the setup on thick $PtSe_2$ FETs and photodiodes. For $PtSe_2$ FETs we identified a limit of our transistors due to their thickness and of our choice of substrate which itself presents a photoresponse. Quartz or Saffire substrates could be better candidates for future device fabrications. Next challenge is to reduce the $PtSe_2$ thickness to reach semiconducting behavior, better suited for the study of photodetectors.

Acknowledgments

I would like to thank a lot my two supervisors Emmanuel Baudin and Marin Tharrault who did an amazing job in making sure my internship would be of the best quality. I had an excellent experience in their company and, eventhough we will not continue working together, I hope them the best in their future projects.

---

[1] F. Cadiz, E. Courtade, C. Robert, G. Wang, Y. Shen, H. Cai, T. Taniguchi, K. Watanabe, H. Carrere, D. Lagarde, M. Manca, T. Amand, P. Renucci, S. Tongay, X. Marie, and B. Urbaszek. Excitonic linewidth approaching the homogeneous limit in mos_2-based van der waals heterostructures. *Phys. Rev. X*, 7:021026, May 2017.

[2] Andres Castellanos-Gomez, Michele Buscema, Rianda Molenaar, Vibhor Singh, Laurens Janssen, Herre S J van der Zant, and Gary A Steele. Deterministic transfer of two-dimensional materials by all-dry viscoelastic stamping. *2D Materials*, 1(1):011002, apr 2014.

[3] Sujay Desai, Surabhi Madhvapathy, Matin Amani, Daisuke Kiriya, Mark Hettick, Mahmut Tosun, Yuzhi Zhou, Madan Dubey, Joel Ager, D. Chrzan, and Ali Javey. Gold-mediated exfoliation of ultralarge optoelectronically-perfect monolayers. *Advanced materials (Deerfield Beach, Fla.)*, 28, 03 2016.

[4] Yuan Huang, Yuhao Pan, Rong Yang, Li-Hong Bao, Lei Meng, Hai-Lan Luo, Yong-Qing Cai, Guo-Dong Liu, Wen-Juan Zhao, Zhou Zhang, Liang-Mei Wu, Zhi-Li Zhu, Ming Huang, Li-Wei Liu, Lei Liu, Peng Cheng, Ke-Hui Wu, Shi-Bing Tian, Chang-Zhi Gu, and Hong-Jun Gao. Universal mechanical exfoliation of large-area 2d crystals. *Nature Communications*, 11, 05 2020.

[5] Joel I-Jan Wang, Yafang Yang, Yu-An Chen, Kenji Watanabe, Takashi Taniguchi, Hugh O. H. Churchill, and Pablo Jarillo-Herrero. Electronic transport of encapsulated graphene and wse2 devices fabricated by pick-up of prepatterned hbn. *Nano Letters*, 15(3):1898–1903, 2015. PMID: 25654184.

[6] Yuda Zhao, Jingsi Qiao, Zhihao Yu, Peng Yu, Kang Xu, Shu Lau, Wu Zhou, Zheng Liu, Xinran Wang, Wei Ji, and Yang Chai. High-electron-mobility and air-stable 2d layered ptse 2 fets. *Advanced Materials*, 29, 11 2016.